CHAPTER II

DESCRIPTION OF APPARATUS AND EXPERIMENTAL TECHNIQUES

2.1. Light sources

2.1.1. Ultraviolet lasers

The ultraviolet laser systems used in the experiments described in Chapter 3 and listed in Table 3.1, covered a broad range of wavelengths and pulse durations. They included a seeded single-mode Nd:YAG laser, a nitrogen laser, and a Ti:sapphire ultrafast laser system. Nanosecond-duration pulses at 266 nm were generated using non-linear crystals to frequency-quadruple the single-mode Nd:YAG laser, while the output of the N_2 laser at 337 nm was used directly. Femtosecond laser pulses were produced from a regeneratively amplified Ti:sapphire laser system that is described in more detail elsewhere [1]. The fundamental 120 fs, 800 nm output was frequency doubled (400 nm) or tripled (266 nm) in non-linear crystals. All of the lasers used except the seeded Nd:YAG have Gaussian spatial intensity profiles; the Nd:YAG has a "top hat" profile produced by a phase conjugating element. The beam profiles are somewhat altered by the 45° projection angle onto the sample.

The mass spectrometer used at Vanderbilt is fitted with an optical port that will accept multiple lasers. A nitrogen laser (337i and 337-Si, Laser Science Inc., Franklin, MA) was often used to find appropriate voltage and timing settings, reducing the amount of valuable FEL time necessary for such tasks, as well as to compare the MALDI mass spectra generated by ultraviolet and infrared irradiation.

2.1.2. Vanderbilt free-electron laser

The Vanderbilt FEL is a rf-linear-accelerator-driven FEL which is continuously tunable from 2 – 10 μm [2]. In the free-electron laser, spontaneous emission is produced by [free-free] transitions as a relativistic electron beam is guided through a region containing a spatially periodic magnetic field called a "wiggler." By properly phasing the maximum amplitudes of the electromagnetic and electron waves, it is possible to create a resonance condition in which the radiative process is enhanced or amplified by classical electromagnetic-field effects [3]. The

wavelength λ_{FEL} of the FEL is related to the energy of the electron beam and the wiggler field by:

$$\lambda_{FEL} = \frac{\lambda_W}{2\gamma^2}\left(1 + \kappa^2\right) \tag{2.1}$$

where λ_W is the wiggler period; γ is the ratio of the electron-beam energy to the electron rest energy; and κ is a magnetic-field-dependent quantity of order unity. Thus the FEL wavelength can be varied continuously over a wide range by changing either the wiggler magnetic field or the electron-beam energy. In practice, variations within ±10% of the nominal frequency are accomplished by opening or closing the gap between the wiggler magnets. Larger frequency shifts are implemented by changing electron-beam energy and where necessary retuning the beam through the wiggler and associated electron optics.

The temporal pulse structure in a free-electron laser is determined by the choice of electron accelerator and rf generation system. In the Vanderbilt FEL, this is an S-band klystron operating at 2.865 GHz; the klystron delivers a 9 μs rf pulse at a maximum pulse repetition frequency of 30 Hz. Each macropulse comprises some $\sim 3 \cdot 10^4$ 0.7-1.0-ps micropulses in a 4-μs macropulse, with an interpulse spacing of 350 ps. Typical macropulse energies are in the range 30-120 mJ. The FEL beam as delivered to the user laboratories exhibits a diffraction-limited TEM_{00} spatial profile; the pulse width of the micropulses is essentially transform-limited. There is a frequency chirp during the macropulse of approximately ±2-3% of the central frequency; however, the switched 100 ns portion used in our experiments contains a much smaller spread in frequency. Tuning the FEL from one frequency to another in a narrow range (±10%) around a central frequency is generally accomplished by adjusting the wiggler magnetic field; larger adjustments of frequency require returning the electron-beam energy and sometimes inserting a new mirror set in the optical cavity to optimize the laser gain.

Because the macropulse duration is much longer than the time scales of interest, broadband electro-optic switch, or Pockels Cell, (II-VI, Inc. Saxonburg, PA) was used to slice a short pulse train (≥100 ns) from the macropulse with a contrast ratio of order 160:1. The duration of the switch is limited by the switching time of the electronics. Since the FEL beam diameter as delivered to our laboratory was larger than the crystal face of the Pockels Cell, a mirror telescope was used to reduce the beam by a factor of three. This required introducing the beam to the first mirror slightly off axis, resulting in a slightly elliptical spot size downstream in

the optical train. The intensity of the beam was controlled by adjusting the relative orientation of two polarizers placed after the Pockels Cell. Our focusing optics, set outside the vacuum chamber in a reentrant flange, typically provided a 100-200 μm diameter spot on the target, which was measured by thermally sensitive paper. The Gaussian beam profile was projected onto the sample at a 45° of incidence, often resulting in an elliptical profile on the sample. One way to avoid the variability in effective spot size with increasing energy inherent with Gaussian beam profiles is to use a sample fiber to provide a top-hat profile. Unfortunately, the high intensity of the FEL micropulses exceeded the damage thresholds of all examined fiber materials to date [4].

Energy measurements were made with Molectron (Portland, OR) detectors (J25 and J3-05) and power meters (EPM 2000).

2.2. Mass spectrometer systems

For UV-MALDI experiments described in Chapter 3, a commercial reflectron TOF (RTOF) (Voyager RP, PerSeptive Biosystems, Framingham, MA) was used, with the TOF extraction plate biased at 20 kV. Delayed extraction was not used in these experiments. All mass spectra were acquired through a digital oscilloscope (Tektronix TDS 520S, Beaverton, OR) and analyzed using the GRAMS/386 data acquisition program (Galactic, Salem, NH). Ions were detected with commercial microchannel plate detectors. Calibration of this mass spectrometer was accomplished with various internal and external standards.

The mass spectrometer in the Vanderbilt FEL lab is a custom-built lab-modified Comstock reflectron time-of-flight mass spectrometer (Comstock, Inc., Oak Ridge, TN). During the four years the instrument has been in our lab, we have never observed the performance one would expect from a dedicated instrument, even upon installation. There has been a group effort to correct a number of egregious design errors including the installation of new focussing optics, ion source and high voltage switch. Recent modeling of ion flight times led several of us to more carefully describe the various components of the system and alter the switching parameters. It now appears that the primary limitations were/are; a spike on the output of the high voltage switch, a poorly designed post acceleration region and the low voltage available on the ion

source. More specific details related to the operation and design of the mass spectrometer are being compiled in a group users' manual.

All data presented here involve ion acceleration in a two-stage ion source by pulsing the voltage on the repeller, grounding the extraction grid and applying a static voltage on the flight tube grid. Earlier experiments used voltages of about 5 kV on the repeller and -4 kV on the flight tube, creating fields of 417 and 500 V/mm in the extraction and acceleration regions, respectively. After improvements were made to the high voltage switch, which resulted in a longer rise time but a shorter spike on the leading edge, the voltage applied to the repeller was typically about 1 kV, while the flight tube was typically held at –5 kV. The ions were allowed to accelerate for a period of time before extraction, between 300-800 ns, depending on the mass of the analyte being studied. Ion signals were observed with a dual microchannel plate detector, routed through a fast digitizer (PDA500, Signatec, Corona, CA), recorded and analyzed on a microcomputer. Schematics for the reflectron, post-acceleration region and ion mirror are found at the end of this chapter in Figures 2.2-2.4, respectively.

2.3. Materials and sample preparation

The sample preparations for the experiments described in Chapter 3 are described in Section 3.2. The polycarboxylic acids used in the studies described in Chapter 4 were chosen because of their importance in hazardous tank waste [5]. The tank waste simulant included sodium nitrate, chelators originally added to the waste - HEDTA (N-(2-Hydroxyethyl)ethylenediaminetriacetic acid), EDTA (ethlyenediaminetetraacetic acid), NTA (nitrilotriacetic acid) and citric acid - and several small carboxylic acids that are degradation products of these chelants, shown in Figure 4.1. These compounds were purchased from Sigma-Aldrich (St. Louis, MO), while $NaNO_2$, $NaNO_3$, NaOH and NH_4OH were purchased from Fisher Scientific (Suwanee, GA). All chemicals were used as purchased without further purification. Samples were made by dissolving the compounds in 2.0 M $NaNO_3$ solutions, depositing several μL of the solution on a steel microtiter plate and then drying the sample under a stream of warm air, producing a thin film of microcrystallites. A pH meter (Accumet pH meter 915, Fisher Scientific, Houston, TX) was used to monitor the pH of the samples.

The analyte:matrix molar ratios used in this study (1:20-80) were chosen to address the concentrations relevant to the tank waste aging problem. This is quite different from the ratios used for MALDI as practiced for large biomolecules, which are typically 1:1000 or lower. However, these ratios have been found to be better for low molecular weight compounds, which likely reflects the role of the matrix either in transporting the analyte molecules into the gas phase or for optimizing charge transfer between matrix molecules and analyte surface sites [6].

The samples used in the wavelength scans described in Chapter 5 were prepared from a mixture of 150 μL of 200 mM succinic acid in methanol and 3 μL of 1 mM neurotensin in 0.1% TFA, resulting in a 10^4:1 matrix:analyte molar ratio. Several μL of the sample was placed on the stainless steel substrate and dried under a stream of cool air.

2.4. Fourier transform infrared spectroscopy

Two methods were used to measure the infrared absorption spectra of compounds in this work, both using Fourier transform infrared spectroscopy (FTIR). One involved measuring the compound as a dilute component in KBr, an IR-transparent material, which allowed for the determination of the molar decadic coefficient, and thus laser penetration depth in the material. The compound was mixed at an appropriate concentration in KBr that had been finely ground and dried, typically for greater than twenty-four hours in an oven at 110°C. After drying, the mixture was removed from the oven and then ~200 mg were placed in a die and pressed under a pressure of 1 GPa. The resulting disk was measured in transmission mode of a Mattson FTIR spectrometer spectrometer (Mattson Instruments, Madison, WI). Care was taken to keep the compound concentration low enough so that the transmission loss of the strongest peak was between 30 - 60%, avoiding potential instrument saturation. For the measurement of 2,5-DHB and succinic acid, concentrations of about 1% (mass concentration) in KBr were used. Two preparations of $NaNO_3$ were needed for the two wavelength regions of interest to result in the desired transmission losses; a concentration of ~0.005% at the nitrate stretching mode and a concentration of 0.1% at the overtone. An undoped KBr disk was also prepared and used as the background to account for losses due to surface reflection. However, since transmission losses are due to both absorption and scattering, the calculated penetration depths from the sample

absorbance under-represent the actual value. The molar decadic coefficients, ε_n at all wavelengths were calculated on a spreadsheet using the following equation:

$$\varepsilon_n = \frac{A}{ct} \tag{2.2}$$

where A is the absorbance, c is the sample concentration (mol/L), and t is the pellet thickness (cm). The 1/e penetration depth in the sample is then found according to the equation:

$$d_e = \frac{1}{2.3\varepsilon_n c} \tag{2.3}$$

The mid-IR absorption profile of samples prepared as used in experiments was measured by attenuated total reflectance (ATR) spectroscopy with a FTIR spectrometer (66-v Bruker Instruments, Bremen, Germany). ATR FTIR probes the surface of the sample with the evanescent wave of the IR beam to a depth of about λ/10 by multiple reflections along the length of IR transparent material with a high index of refraction. In this case a ZnSe crystal was used as the substrate, and the sample was applied directly to the surface of the crystal as a solution and then dried with a stream of warm air.

Table 2.1. Equivalence points and pK_a values for HEDTA determined by titration

	HEDTA	HEDTA+SN -1	HEDTA+SN -2	Lit. values
pK_1	2.66	2.64	2.5	2.39
pK_2	5.47	5.58	5.46	5.37
pK_3	9.98	9.25	9.38	9.93
EP 1	3.95	3.81	3.80	
EP 2	7.62	7.16	7.19	
EP 3	10.97	10.30	10.62	

2.5. Titration measurements

Titration measurements were performed to determine the equivalence points (EP) of the carboxylic acids used in the studies of the effect of initial pH on the observed ions in the mass

spectra. The equivalence point is the pH at which a labile proton is completely dissociated, and therefore allows one to predict the charge state of the molecule in solution. The carboxylic acids were present in a 2 M solution of sodium nitrate, so it was necessary to measure the EPs in that environment rather than rely on literature values, since the presence of nitric acid shifted the EPs to lower pH values. The EP values of the polycarboxylic acids were measured both with and without sodium nitrate, the latter to compare the results of the experimental technique with

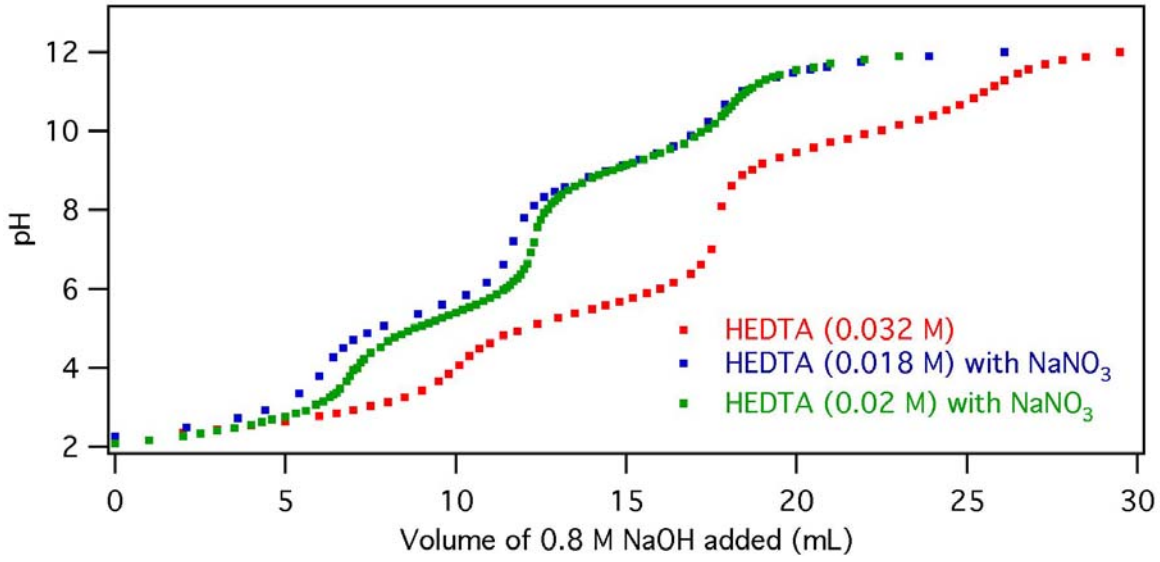

Figure 2.1. Titration curves for HEDTA in water (red) and aqueous sodium nitrate (blue and green). Values for the pK_a values and equivalence points are found in Table 2.1.

literature values. Sodium hydroxide was used as the titrant at values between 0.5 and 1.0 M for the various experiments, while the 0.02-0.1 M polycarboxylic acids were added either to H_2O or 2.0 M sodium nitrate. A pH meter (Accumet pH meter 915, Fisher Scientific, Houston, TX) was used to monitor the pH of the samples – indicators were not used. Sample data of the titration curves for the polyprotic HEDTA are shown in Figure 2.1, and the measurements of the pK_a values and equivalence points (EP) are given in Table 2.1. The three curves represent three separate titrations, one in water (HEDTA) and two in aqueous sodium nitrate (HEDTA+SN–1,2) to determine repeatability. Literature values ('Lit. values' in the table) for the pK_a values are also included. The experimentally determined pK_a values were within 0.3 of the literature values for HEDTA in aqueous solution, and the EP values for the two trials of HEDTA in sodium

nitrate solutions were within 0.32 of each other. The EPs of glycolic acid and oxalic acid are reported in Table 4.2.

2.6. Computational determination of sodium gas-phase affinities

The structures of three carboxylic acids as were modeled with density functional theory at the B3LYP level followed by vibrational analysis to calculate the sodium binding energies. Geometries for the bare neutral, mono- and di-salt forms were first optimized, and then several possible structures for a sodium cation were queried. The zero-point vibrational energies were determined, and thermal corrections were made using the vibrational analysis to obtain the binding energies at 298 K. Binding entropies were also obtained to derive binding free energies. The data presented here represent first-run results, and the values should be viewed primarily to denote differences in structures, as further optimization may slightly alter the exact values.

BIBLIOGRAPHY

[1] W. P. Hess, A. G. Joly, K. M. Beck, R. M. Williams, and J. T. Dickinson, Applied Physics A-Materials Science & Processing **69** (7), S389 (1999).

[2] G. S. Edwards, D. Evertson, W. Gabella et al., IEEE J. Sel. Top. Quantum Electron. **2**, 810 (1996).

[3] C. A. Brau, *Free-Electron Lasers*. (Academic Press, New York, 1990).

[4] S Ullhorn (personal communication).

[5] A. K. Sharma, S. A. Clauss, G. M. Mong, K. L. Wahl, and J. A. Campbell, J. Chromatogr., A **805**, 101 (1998).

[6] Richard Knochenmuss, Volker Karbach, Ursula Wiesli, Kathrin Breuker, and Renato Zenobi, Rapid Communications in Mass Spectrometry **12** (9), 529 (1998).

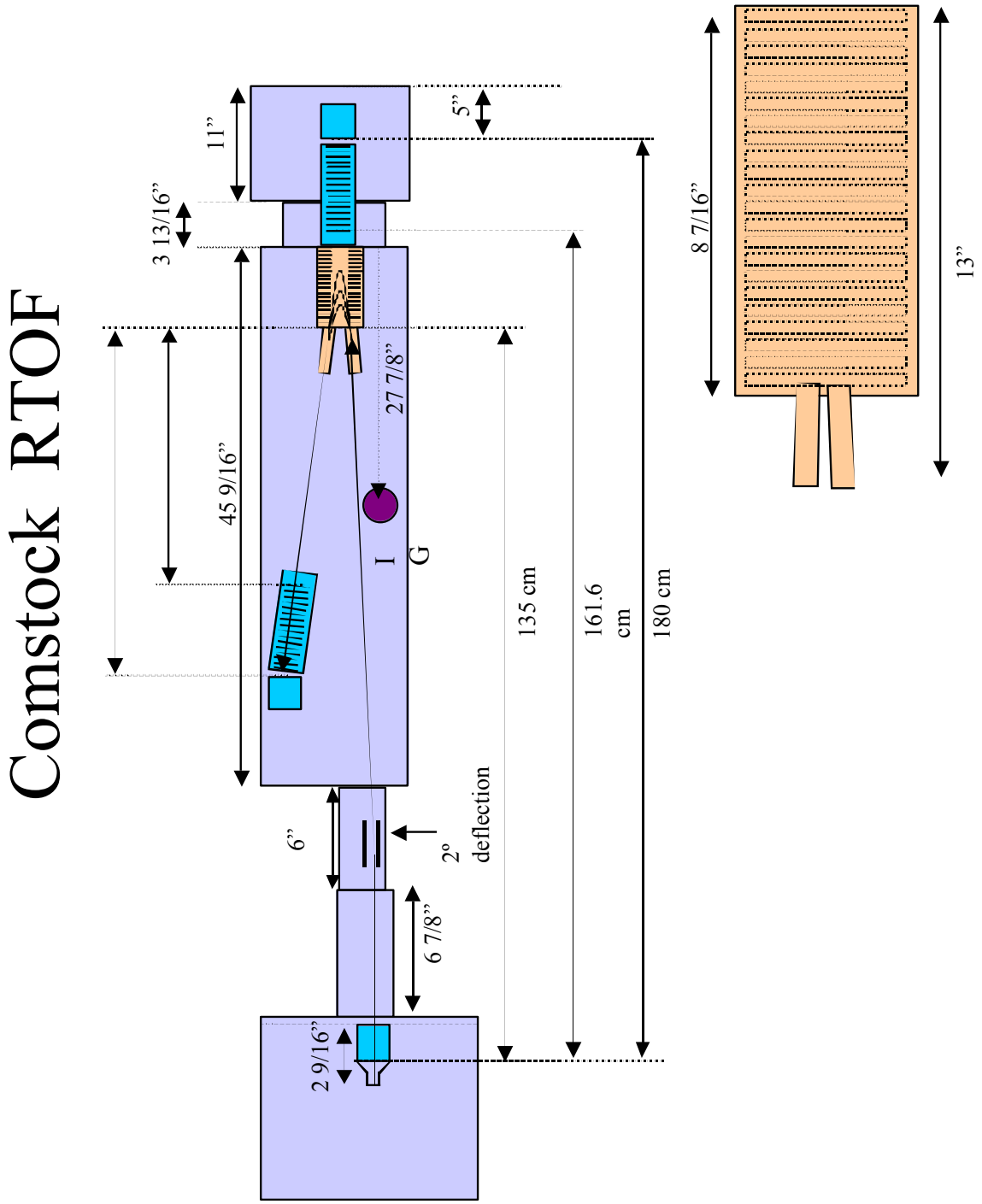

Figure 2.2 Rough schematic of the Comstock reflectron mass spectrometer

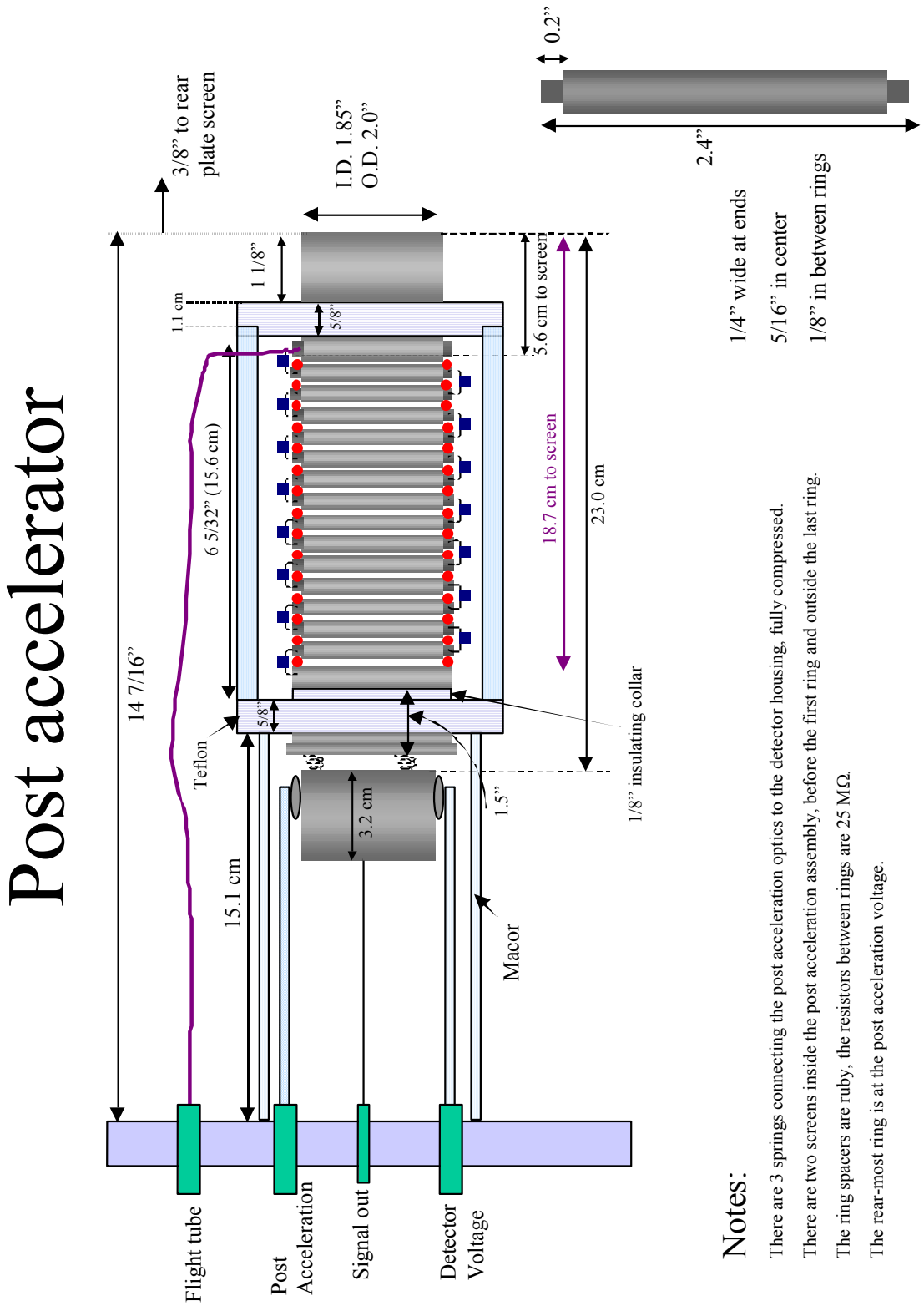

Figure 2.3. Schematic of the post acceleration region

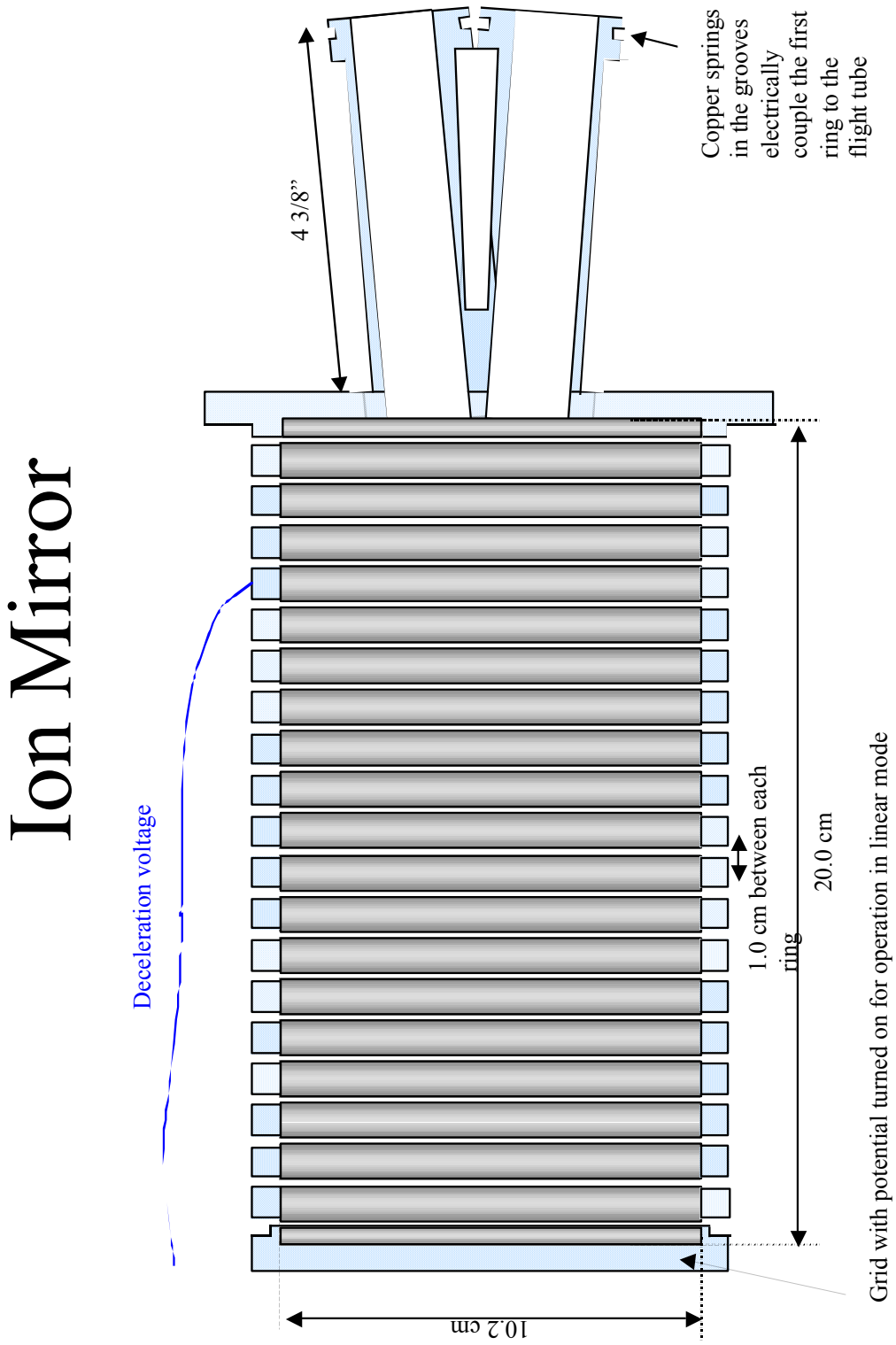

Figure 2.4 Schematic of the ion mirror used in the Comstock mass spectrometer.